ELSEVIER

Contents lists available at ScienceDirect

Ceramics International

journal homepage: www.elsevier.com/locate/ceramint





Effect of various morphology of in situ generated NbC particles on the wear resistance of Fe-based cladding

Wenchao Xi ^{a,b}, Boxue Song ^c, Zhengyu Sun ^a, Tianbiao Yu ^{a,*}, Jun Wang ^a, Qi Sun ^{b,c}

- ^a School of Mechanical Engineering and Automation, Northeastern University, PR China
- ^b School of Mechanical and Aerospace Engineering, Nanyang Technological University, Singapore
- ^c School of Mechanical Engineering, Shenyang University of Technology, PR China

ARTICLE INFO

Keywords:
In situ
NbC particles
Morphology
Wear mechanism
Wear resistance

ABSTRACT

To improve the wear resistance of Fe-based cladding, NbC particles with different morphology are generated in situ by adding Nb, Cr_3C_2 and C with different content. The composition of samples and the morphology of NbC particles generated in situ are revealed by XRD, SEM and EDS. The wear resistance is studied by a reciprocating friction and wear testing machine. The wear mode and the wear mechanism of each sample are investigated. The results show that although NbC particles are generated in situ in samples with different Nb, Cr_3C_2 and C content, the morphology of NbC particles is varied. The wear resistance of samples containing cross-shaped NbC particles is more outstanding than that of samples containing only rectangular NbC particles. In addition, changing Nb, Cr_3C_2 and C content does not result in a change in wear mode, but leads to the formation of continuous lattice structure of $Cr_{0.19}Fe_{0.7}Ni_{0.11}$ and $Cr_{23}C_6$ compounds at grain boundaries and a change in the wear resistance. When the additions of Nb, Cr_3C_2 and C are 11.2 wt%, 8.6 wt% and 0.2 wt% respectively, the coefficient of friction of the sample is the lowest, and the wear resistance is the most outstanding.

1. Introduction

NbC is a cermet with high hardness, high melting point, good chemical stability and high temperature properties [1-3]. However, due to its scarcity, high cost and inherent brittleness, NbC is difficult to be proceeded into workpieces with large volume and high purity [4,5]. In view of this, NbC is mixed with low-cost powders to form cladding with outstanding properties on the surface of the substrate by directed energy deposition [6-8]. Currently, the technique has attracted more and more attention and obtained some achievements.

Li et al. [9] investigated the relationship between the NbC content and the properties of high-entropy alloy (Fe50Mn30Co10Cr10) coating. The results showed that the nano-NbC particles inhibited the growth of dendritic crystals and increased the nucleation rate of the grains. It resulted in a decrease of columnar grains and an increase of equiaxed grains, which improved the properties of the coating. However, the distribution of NbC particles was not uniform when the NbC content was 10 wt% or 20 wt%. Wang et al. [10] added different content of NbC to Ti–Al–Si coatings, and the results showed that a part of the added NbC decomposed and formed (Ti, Nb)C with Ti in the coating. When NbC

content reached 15%, the hardness of the coating was three times that of the substrate. Li et al. [11] confirmed that the addition of NbC inhibited the formation of FCC phase and promoted the transformation of FCC phase to BCC phase in the high-entropy alloy coating, and the results showed that the higher the addition of NbC, the more outstanding the mechanical properties. Zhang et al. [12] proposed that although the addition of NbC can effectively improve the wear resistance, excessive NbC can lead to an increase in the local brittleness, resulting in a deterioration of the wear resistance of coating. In summary, the mechanical properties can be significantly improved by adding NbC particles to the coating, but a part of the NbC particles are not completely melted due to the rapid rate of melting and solidification during the laser cladding. During the wear process, the incompletely melted NbC particles are spalled off and spallation pits are formed, resulting in an increase in the surface roughness and the coefficient of friction. In addition, spalled NbC particles can damage the coating surface and lead to increased wear rates [13]. In order to avoid this phenomenon, an attempt has been made to replace the direct addition of NbC to the coating by in situ formation of NbC particles in the coating.

Li et al. [14] demonstrated that regular NbC particles can be in situ

^{*} Corresponding author. NO. 3-11, Wenhua Road, Heping District, Shenyang, PR China. E-mail addresses: neu_wenchaoxi@163.com (W. Xi), bamboomoon.harold@gmail.com (B. Song), wayne0112@163.com (Z. Sun), neutianbiaoyu2018@gmail.com (T. Yu), 363825394@qq.com (J. Wang), sunqi6126@163.com (Q. Sun).

generated by adding Nb and C to the coating, and confirmed that an increase in the NbC content leads not only to an increase in the porosity, but also to changes in the shape, amount and size of the NbC particles. Cai et al. [15] pointed out that with the increase of NbC content, the coefficient of friction and wear rate decreased, and confirmed that NbC particles generated in situ improved the wear resistance of gray cast iron significantly. Shi et al. [16] presented that the added Cr₃C₂ all decomposed and formed Cr23C6 and Cr7C3. However, the added Nb was not completed dissolved. In addition, the $Cr_{23}C_6$ and Cr_7C_3 also served to improve the mechanical properties of the coating. Ping et al. [17] confirmed that NbC particles can also be in situ generated by adding Nb to the Ni60A-Cr₃C₂ coating, and that the size and volume fraction of NbC particles increased with the addition of Nb. When the addition of Nb was 3 wt%, the wear resistance reached 2.3 times that of the Ni60A-Cr₃C₂ coating. Wang et al. [18] demonstrated that NbC particles can be in situ generated by adding Nb and B₄C to the coating, and that Fe₂B was also in situ generated in the coating. The wear resistance is increased by a factor of 1.5 in the effect of NbC and Fe₂B. Cao et al. [19] pointed out that not all of the Nb and C added to the coating reacted in situ, and that about one-third of the Nb was exist as solid solution. Zhang et al. [20] prepared NbC in the WCoB-TiC composite coating. The results showed that the addition of Nb significantly improved the microhardness of the coatings, although Nb led to an increase in dilution rate and porosity. Lu et al. [21] confirmed that the in situ formation of NbC particles acted as a pinning effect to inhibit the growth of grains, thus achieving a grain refinement effect. The interlayer bonding strength was improved by the effect of fine grain strengthening. Dong et al. [22] presented that NbC particles were in situ generated by adding different content of Nb to the Ni-based alloy composite coating. Meanwhile, the addition of Nb inhabited the formation of M7C3 carbides, thus improving the wear resistance of the coating. Yang et al. [23] confirmed that NbC particles can be in situ generated by adding different content of Nb to Fe-Cr-C coatings. As the Nb content increased, the martensite was refined. As a result, the hardness, tensile strength and yield strength are improved.

In summary, NbC particles can be in situ generated by adding Nb combined with C or Cr₃C₂ into the cladding, but the morphology of the generated NbC particles changed with the content of Nb, C and Cr₃C₂. Meanwhile, although Nb and C are added to the cladding in a 1:1 atomic mass ratio, still nearly one-third of the Nb did not react with C in situ but existed in the cladding as a solid solution. In order to generate more NbC particles in situ and to investigate the effect of the morphology of the NbC particles generated in situ on the wear resistance of cladding, NbC particles with different content and morphology were generated in situ by adding different content of Nb, C and Cr₃C₂. Then, the composition of each sample was revealed by XRD, and the morphology of NbC particles in each sample was analyzed and studied by SEM and EDS. Finally, the effect of different morphology of in situ generated NbC particles on the coefficient of friction, wear rate, wear mode and wear resistance were investigated, and the wear mechanisms of in situ generated NbC particles reinforced cladding with different morphology was analyzed.

2. Experimental details

2.1. Directed energy deposition

The directed energy deposition testing machine used in this test consists of: a continuous wave laser generator (spot diameter: 1.1 mm), a powder feeding system, a cooling system and a vertical machining center (VMC 1100P) as shown in Fig. 1. In this case, the deposition head is installed on the vertical machining center in order to ensure precise movements in X, Y and Z directions. The powder is injected into the laser beam through a coaxial powder feed nozzle. Both the powder feeding gas and the shielding gas are argon gas with a purity of 99.99%. The flow rate of the shielding gas is 15 L/min. To ensure that the intersection of powder flow is at the substrate surface, the distance between the nozzle and the substrate surface is a fixed value of 16 mm.

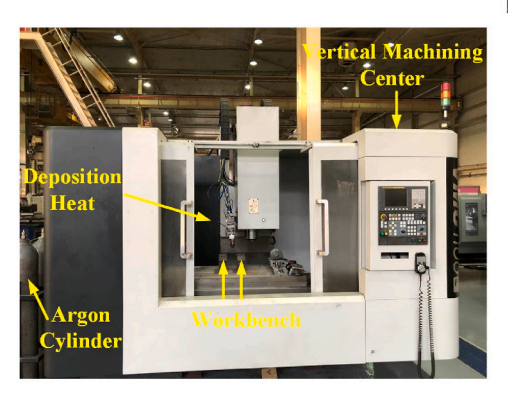






Fig. 1. Directed energy deposition testing machine.

The material of substrate is AISI 1045 steel with the composition shown in Fig. 2(b). Before directed energy deposition tests are carried out, the substrate surfaces are grinded by metallurgical sandpaper to remove debris and make the surfaces of the substrate flat. Then, the substrates are ultrasonically cleaned in ethanol absolute to remove the stains from the surfaces of the substrates. Finally, the substrates are dried by a drying baker for 30 min.

YCF102 powder is a type of spherical Fe-based powder with a grain size of 100 mesh to 270 mesh, and its composition is shown in Fig. 2(a). YCF102 powder is used as the test powder due to its good compatibility with AISI 1045 steel and the easy formation of a good metallurgical bond with the substrate. Both Nb and Cr_2C_3 powders are irregular powders with a grain size of 100 mesh to 150 mesh, and the purity is 99.5%. The carbon black powder (\geq 100 mesh) is an irregular powder produced by Aladdin. The above powders are mixed in different proportions by a ball mill mixer, and the composition of mixed powders is shown in Table 1. In this case, the material of the mixing ball is aluminum oxide and the mass ratio of mixing ball to powder is 2:1.

According to the authors' previous study [24], the cladding possesses satisfactory geometry and defect number when the laser power is 750 W, the scanning velocity is 4 mm/s, and the powder feeding rate is 7 g/min. Therefore, the above process parameters are used in this work.

2.2. Reciprocating friction and wear tests

After the deposition, the cladding is cut into samples with a size of 25 mm (Length) \times 10 mm (Width) \times 10 mm (Thickness) by wire electrical discharge machining, and the surface of samples is grinded by metallographic sandpaper and a polishing machine. The tribological properties of samples are tested by a reciprocating friction and wear tester (MFT-4000), and real-time curves of coefficient of friction are obtained. In this case, the wear velocity is 240 mm/min, the load is 10 N, the wear distance is 5 mm, the diameter of grinding ball is 4 mm and the material of grinding ball is SiN. The wear morphology of samples is obtained by laser confocal.

2.3. X-ray diffraction and scanning electron microscopy

The surface of samples is etched by aqua regia and ultrasonically cleaned by ethanol absolute and deionized water. Then, the samples are dried by a drying baker for 30 min, and the composition and morphology of samples are revealed by X-ray diffractometer (XRD), scanning electron microscope (SEM) and energy dispersive spectroscopy (EDS). To ensure the reliability of the test data, three repeatability tests

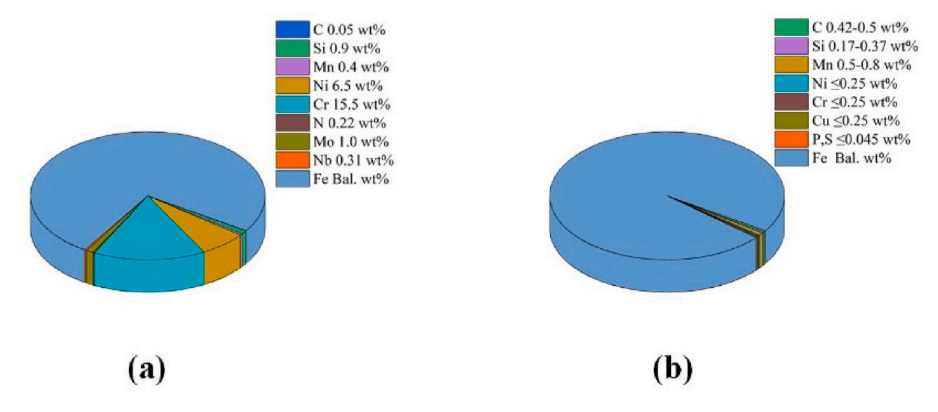


Fig. 2. Composition of (a) YCF102 alloy powder and (b) AISI 1045 substrate.

Table 1
Composition of mixed powder (wt%).

Sample No.	YCF102	Nb	Cr ₃ C ₂	С
1	80	17.8	0	2.2
2	80	10.2	9.8	0
3	80	11.2	8.6	0.2
4	80	11.8	7.6	0.6
5	80	14.2	4.6	1.2

are carried out on each sample under the same conditions.

3. Results and discussion

3.1. The main composition of cladding

Fig. 3 shows the XRD patterns of samples. The main phases of samples are NbC, $Fe_{0.64}Ni_{0.36}$, $Cr_{0.19}Fe_{0.7}Ni_{0.11}$, Fe_2Nb and $Cr_{23}C_6$, indicating that variously mixed Nb, C and Cr_3C_2 powders react in situ and generate NbC. Meanwhile, different content of Fe_2Nb is found. From other research, although Nb and C are added to the cladding in a 1:1 atomic mass ratio, still nearly one-third of the Nb does not react with C in situ [25]. Therefore, the rest of Nb does not react in situ with C, but reacts in situ with Fe in the powder to generate Fe_2Nb . In addition, Cr_3C_2

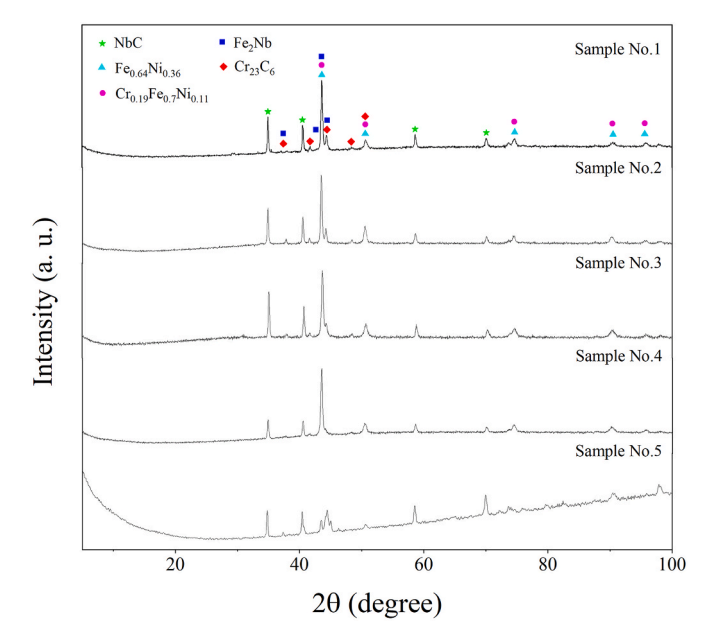


Fig. 3. The XRD pattern of each sample.

is not found, but $Cr_{23}C_6$ is found in samples No.2 to No.5. The results show that $Cr_{23}C_2$ is decomposed during directed energy deposition. The generated C reacts in situ with Nb to generate NbC. $Cr_{23}C_6$ is also found in sample No.1. However, $Cr_{3}C_2$ is not added to sample No.1. It indicates that a part of C reacts in situ with Nb to generate NbC during the directed energy deposition, while another part of C reacts in situ with Cr to generate $Cr_{23}C_6$.

3.2. The cladding morphology

Figs. 4 to 8 show the SEM mapping scanning results for samples No.1 to No.5, and Table 2 shows the EDS analysis results for samples No.1 to No.5. In Figs. 4 to 8 and Table 2, the atomic mass ratio of Nb to C at point A is nearly 1:1, indicating that A is the location where NbC particle is generated in situ in the cladding. Due to the effects of Marangoni and thermal capillary motion, the in situ generated NbC particles do not undergo aggregation, but are distributed uniformly in the cladding. Point B of samples No.1 to No.4 shows high contents of Fe, C and Cr, and low contents of Nb, Ni and Si. Combined with XRD patterns, the content of Cr_{0.19}Fe_{0.7}Ni_{0.11} and Cr₂₃C₆ is much higher than that of NbC, Fe₂Nb and Fe_{0.64}Ni_{0.36} at point B. Si does not react with other elements, but exists as a solid solution in the cladding. As shown in Fig. 8 and Table 2, the Fe and Nb content at point B of sample No.5 is higher than that at point B of samples No.1 to No.4, while the C and Cr content at point B of sample No.5 is lower than that of samples No.1 to No.4. Combined with the morphology at point B of sample No.5, it can be seen that point B is the eutectic phase of Cr_{0.19}Fe_{0.7}Ni_{0.11} and NbC. The reason for this phenomenon is the rapid melting and solidification of the melt pool. Due to its high melting point, NbC particles are first separated out at the grain boundaries during solidification. The above phenomenon leads to the occurrence of composition undercooling and temperature undercooling, resulting in the separation of Cr_{0.19}Fe_{0.7}Ni_{0.11} on the surface of NbC. As a result, the occurrence of heterogeneous nucleation leads to the generation of the eutectic phase of Cr_{0.19}Fe_{0.7}Ni_{0.11} and NbC. Figs. 4 to 7 and Table 2 show that the main elements are Fe, C, Cr and Ni at point C of samples No.1 to No.4. The content of Fe and Ni at point C is significantly higher than that at point A and point B. Combined with the XRD patterns, it shows that the main compounds are Cr_{0.19}Fe_{0.7}Ni_{0.11}, Fe_{0.64}Ni_{0.36} and Cr₂₃C₆ at point C. Fig. 8 and Table 2 show that the main element composition of sample No.5 contains not only Fe, C, Cr and Ni, but also Nb at point C. It contains not only $Cr_{0.19}Fe_{0.7}Ni_{0.11}$, $Fe_{0.64}Ni_{0.36}$ and Cr₂₃C₆, but also NbC at point C of sample No.5.

Figs. 4 to 8 and Table 2 show that the morphology of NbC particles in different samples is not the same. The morphology of NbC particles in the sample No.1 is rectangular. Sample No.2 contains a large number of cross-shaped and petal-shaped NbC particles as well as a small number of rectangular NbC particles. The morphology of NbC particles in the sample No.3 is rectangular, cross-shaped and petal-shaped. Sample No.4 contains a large amount of rectangular NbC particles. Flocculent NbC

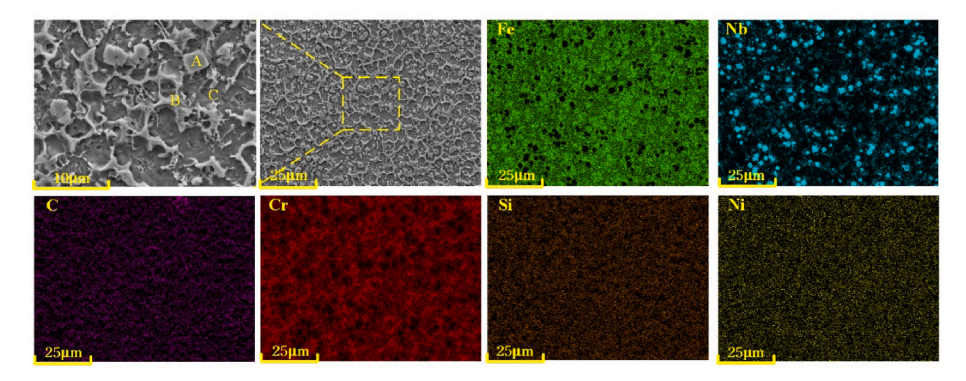


Fig. 4. SEM mapping scanning result of sample No.1.

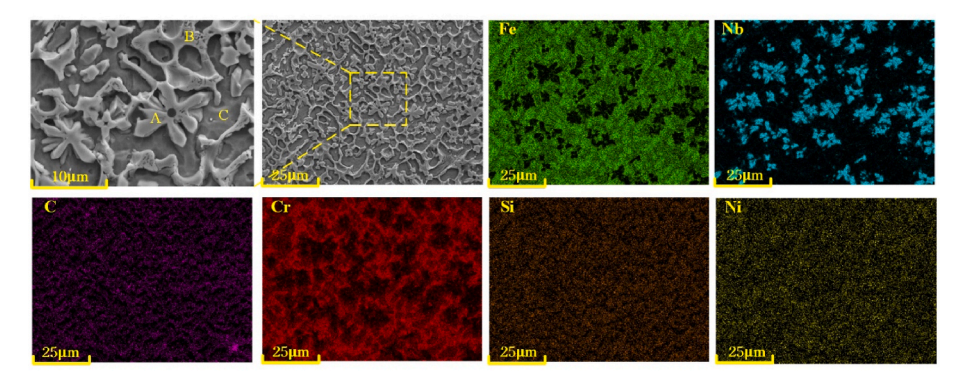


Fig. 5. SEM mapping scanning result of sample No.2.

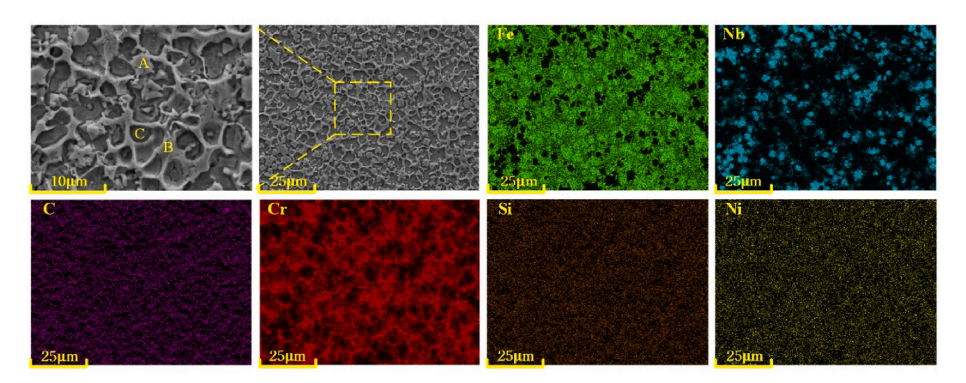
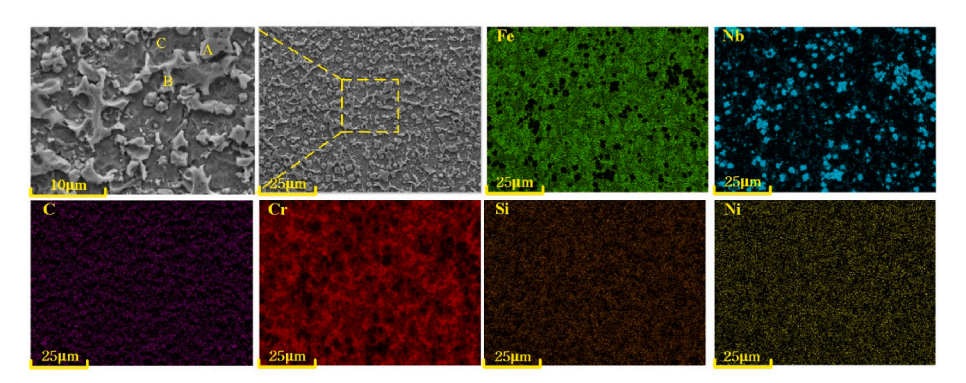


Fig. 6. SEM mapping scanning result of sample No.3.



 $\textbf{Fig. 7.} \ \ \textbf{SEM} \ \ \textbf{mapping scanning result of sample No.4.}$

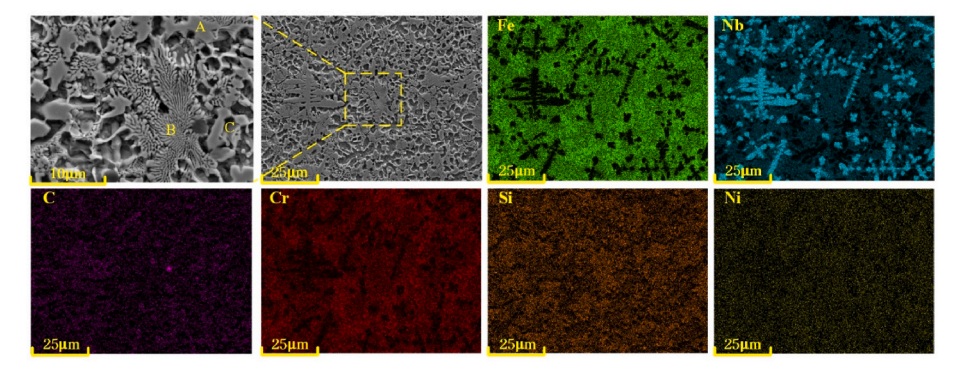


Fig. 8. SEM mapping scanning result of sample No.5.

Table 2
EDS analysis results of various samples (wt%).

		Fe	Nb	С	Cr	Si	Ni
Sample No.1	Α	2.3	48.3	45.9	3.5	0.0	0.0
	В	33.2	1.6	33.8	29.7	0.0	1.7
	C	64.3	0.3	8.1	20.7	1.4	5.2
Sample No.2	Α	1.9	37.8	58.6	1.7	0.0	0.0
	В	38.6	1.9	32.4	25.1	0.5	1.5
	C	72.8	0.5	2.4	17.8	0.8	5.7
Sample No.3	Α	2.0	47.6	46.7	3.7	0.0	0.0
	В	44.8	2.4	21.1	29.9	0.6	1.2
	C	67.8	0.4	4.7	20.0	1.4	5.7
Sample No.4	Α	2.1	48.1	46.7	3.1	0.0	0.0
	В	38.3	0.3	24.5	34.2	0.0	2.7
	C	57.6	0.3	14.0	21.6	1.4	5.1
Sample No.5	Α	7.1	67.6	22.6	2.2	0.5	0.0
	В	50.8	18.0	14.5	8.6	4.0	4.1
	С	53.9	8.6	19.1	12.4	0.9	5.1

particles are found at the grain boundaries of sample No.1 to No.4. Sample No.5 contains a large amount of NbC particles with dendritic structure and a small amount of rectangular and cross-shaped NbC particles. The eutectic phases of NbC and $Cr_{0.19}Fe_{0.7}Ni_{0.11}$ with dendritic structure are found at the grain boundaries of sample No.5.

The different morphology of the in situ generated NbC particles in samples is caused by the changes in the NbC content. Direct energy deposition is a process of rapid melting and solidification. Due to its high melting point, NbC particles are first precipitated. Meanwhile, NbC particles are uniformly distributed in the cladding by Marangoni and thermal capillary motion. NbC is a face-centered cubic structure. When the content of NbC is low, the morphology of NbC particles is rectangular. As the content of NbC increases, the interfacial energy of the {1 0 0} crystal face is lower, which results in a greater growth rate of NbC particles in the {1 0 0} crystal face direction than that in the other directions. The pits appear in the center of the surface due to the large

amount of supercooling at the edge angle, which results in a change in the morphology of NbC particles from rectangle to cross. With a further increase in the content of NbC, NbC particles simultaneously grow in different directions. The morphology of NbC particles changes from cross to petaling [25]. In addition, due to their high melting point, NbC particles are first separated out at the grain boundaries during solidification. The precipitation of NbC particles at the grain boundaries may lead to not only the occurrence of composition undercooling and temperature undercooling, but also the occurrence of heterogeneous nucleation. As a result, the eutectic phase of Cr_{0.19}Fe_{0.7}Ni_{0.11} and NbC is generated at the grain boundaries of Sample No.5.

3.3. The wear resistance of cladding

Fig. 9 shows the coefficient of friction curves for various samples. The coefficient of friction increases to a maximum in the initial stage of wear between samples and the grinding ball, and then decreases gradually to the stable state. When the coefficient of friction fluctuates greatly, the samples are in a state of severe wear. As the wear is performed, the fluctuation amplitude of the coefficient of friction curves decreases gradually and remains in a stable state. It shows that the samples change from a state of severe wear to a state of stable wear. The coefficient of friction in a state of stable wear shows the wear resistance of the samples is better than that in a state of severe wear. Therefore, the coefficient of friction with wear time period of 30–40 min is selected to analyze and study the wear resistance.

In Fig. 9(b), the average coefficient of friction of each sample is in the following order: Sample No.3 < Sample No.5 < Sample No.2 < Sample No.1 < Sample No.4. The reason for this phenomenon is that $Cr_{0.19}Fe_{0.7}Ni_{0.11}$ and $Cr_{23}C_6$ compounds generated at the grain boundaries of sample No.4 do not generate lattice structures, which results in worse wear resistance of sample No.4. The morphology of NbC particles in sample No.2 is the cross-shaped and petal-shaped, while the morphology of NbC particles in sample No.1 is rectangular. According to

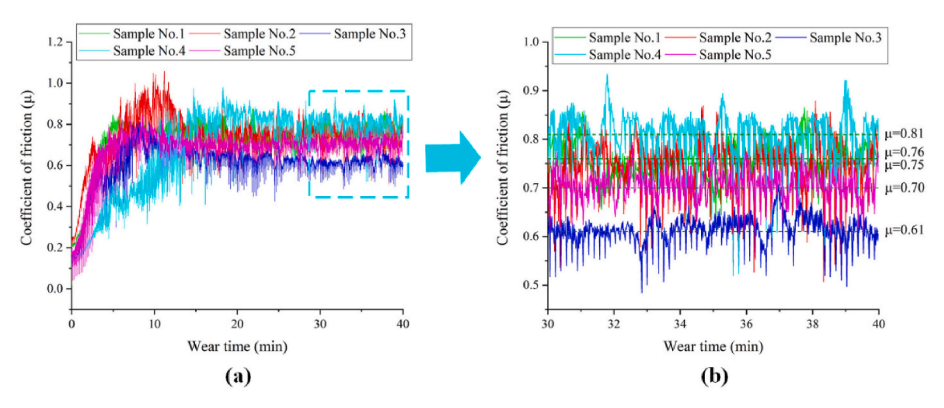


Fig. 9. Coefficient of friction curves of various samples of (a) 0-40 min and (b) 30-40 min...

the other research, when the concentration of NbC is high enough, NbC particles grows from rectangular to cross-shaped and petal-shaped [25]. It indicates that the concentration of NbC in sample No.2 is higher than that in sample No.1, which leads to more outstanding wear resistance of sample No.2 than that of sample No.1. The occurrence of composition undercooling and temperature undercooling leads to the occurrence of heterogeneous nucleation at the grain boundaries of sample No.5. The occurrence of heterogeneous nucleation leads to not only an increase in the nucleation rate but also the precipitation of a large number of the eutectic phase of Cr_{0.19}Fe_{0.7}Ni_{0.11} and NbC at the grain boundaries. As a result, sample No.5 has a lower coefficient of friction and more outstanding wear resistance than sample No.2. Sample No.3 forms continuous lattice structure of Cr_{0.19}Fe_{0.7}Ni_{0.11} and Cr₂₃C₆ compounds at the grain boundaries, and the cross-shaped and petal-shaped NbC particles of sample No.3 are finer than those of other samples. Therefore, sample No.3 has the lowest coefficient of friction and the most outstanding wear resistance.

In summary, the coefficients of friction of samples containing cross-shaped and petal-shaped NbC particles are lower than those of samples containing only rectangular NbC particles, and the wear resistance of samples containing cross-shaped and petal-shaped NbC particles are more outstanding than those of samples containing only rectangular NbC particles. The coefficient of friction of sample No.3 is 24.69% lower than that of sample No.4. Meanwhile, a large number of the eutectic phases of $Cr_{0.19}Fe_{0.7}Ni_{0.11}$ and NbC are precipitated at the grain boundaries of sample No.5, which results in the enhancement of wear resistance. However, due to the fine grain strengthening and the formation of continuous lattice structure of $Cr_{0.19}Fe_{0.7}Ni_{0.11}$ and $Cr_{23}C_6$ compounds at the grain boundaries, sample No.3 has the most outstanding wear resistance.

Fig. 10 shows the wear width, wear depth and wear rate of various samples respectively. The wear width, wear depth and wear rate of various samples are in following order: Sample No.3 < Sample No.5 < Sample No.2 < Sample No.1 < Sample No.4. It is noted that the changing trends of wear width, wear depth and wear rate are the same as that of the coefficient of friction. The wear width, wear depth and wear rate of sample No.3 are minimum, while the wear width, wear depth and wear rate of sample No.4 are maximum. Compared with sample No.4, the wear width, wear depth and wear rate of sample No.3 decrease by 23%, 62% and 46% respectively. The results show that by changing the content of Nb, C and Cr₃C₂, not only can the coefficient of friction, wear width, wear depth and wear rate be effectively reduced, but also the wear resistance can be significantly improved.

3.4. The wear morphology of cladding

Fig. 11 shows the wear morphology of various samples. As can be seen from Fig. 11, a large number of spallation pits and a small number of grooves parallel to the wear direction are found on the wear

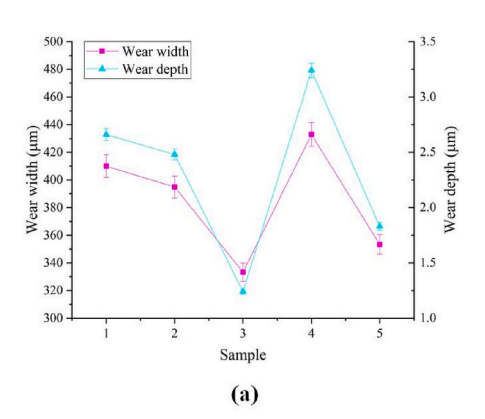
morphology of samples No.3 and No.5, and the grooves parallel to the wear direction on the wear morphology of samples No.1, No.2 and No.4 are significantly more and deeper than those of samples No.3 and No.5. Meanwhile, large spallation pits are found on the wear morphology of samples No.1, No.2 and No.4.

The friction occurs between surface asperities and grind ball during the wear process, which results in the wear surface to be in an alternating state of tensile stress and compressive stress [26]. As a result, spallation pits and chips are formed [27]. Meanwhile, a portion of NbC particles is spalled off due to the fact that the binding force between NbC particles and the cladding is weaker than that of other parts. During the wear process, a part of grinding ball is embedded in the cladding under the action of normal load, and micro-cutting occurs under the action of reciprocating motion. The micro-cutting phenomenon leads to the cutting off of some NbC particles and the generation of chips. A part of chips and spalled NbC particles are accumulated at the ends of the wear track by the reciprocating motion, while another part of the chips and spalled NbC particles roll and slide between the grind ball and the wear surface, which resulting in the formation of grooves [28]. Therefore, the main wear modes are three-body abrasive wear and surface fatigue wear.

It can be seen from Fig. 11 that the change in Nb, C and $\rm Cr_3C_2$ content does not lead to a change in the wear mode, but does lead to a change in the depth and number of grooves and spallation pits. Meanwhile, it can be seen from Fig. 11(a) to 11(e), the wear width of sample No.3 is significantly smaller than that of the other samples. It is indicated that the volume of grinding ball embedded in sample No.3 is the smallest, and the resistance to plastic deformation of sample No.3 is more outstanding than that of other samples. The results show that changes in the morphology of NbC particles do not lead to changes in the wear mode, but do lead to changes in resistance to plastic deformation and wear resistance of cladding.

4. Conclusions

- (1) Although the content of Nb, C and Cr₃C₂ in the mixed powder is changed, NbC particles generated in situ are found in each sample. However, the content of NbC in each sample is different, which leads to different morphology of NbC particles in each sample.
- (2) When additions of Nb, Cr_3C_2 and C are 14.2 wt%, 4.6 wt% and 1.2 wt% respectively, dendritic eutectic phases of $Cr_{0.19}Fe_{0.7}Ni_{0.11}$ and NbC are precipitated at the grain boundaries.
- (3) The Change in the morphology of NbC particles leads to the changes in the coefficient of friction, wear rate and wear morphology, but does not lead to the change in wear mode. During the wear process, all samples undergo three-body abrasive wear and surface fatigue wear.



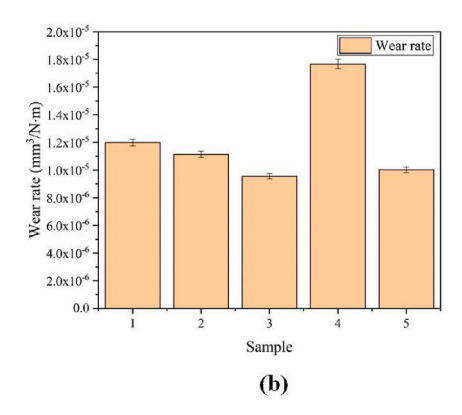
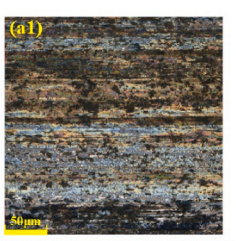


Fig. 10. (a) Wear width and wear depth, (b) wear rate.



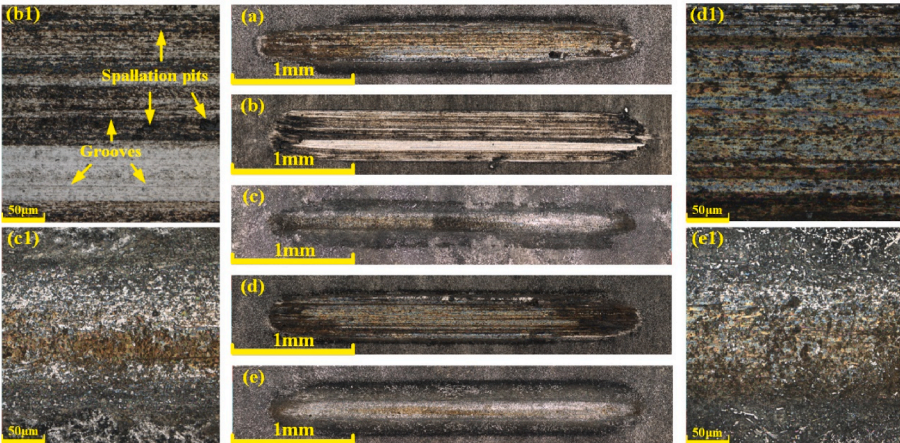


Fig. 11. Worn surface of (a) sample No.1, (b) sample No.2, (c) sample No.3, (d) sample No.4, (e) sample No.5; local enlargement of worn surface of (a1) sample No.1, (b1) sample No.2, (c1) sample No.3, (d1) sample No.4, (e1) sample No.5.

(4) As the content of NbC increases, the morphology of NbC particles changes from rectangular to cross-shaped and petal-shaped. The coefficient of friction of sample No.3 is 24.69% lower than that of sample No.4. The wear resistance and resistance to plastic deformation of the sample containing cross-shaped and petalshaped NbC particles are better than those of the sample containing only rectangular NbC particles.

Credit authorship contribution statement

Wenchao Xi: Conceptualization, Investigation, Writing - Original Draft, Writing - Review & Editing. Boxue Song: Validation, Writing - Review & Editing. Zhengyu Sun: Validation, Writing - Review & Editing. Tianbiao Yu: Resources, Supervision, Project administration, Funding acquisition. Jun Wang: Resources, Supervision. Qi Sun: Writing - Review & Editing.

Declaration of competing interest

The authors declare that they have no known competing financial interests or personal relationships that could have appeared to influence the work reported in this paper.

Acknowledgments

This work is supported by 2016 Green Manufacturing System Integration Project of Ministry of Industry and Information Technology of China [grant number 201675514]; Liaoning Provincial Key Laboratory of Large Equipment Intelligent Design and Manufacturing Technology [grant number 18006001].

References

[1] S.G. Huang, K. Vanmeensel, H. Mohrbacher, M. Woydt, J. Vleugels, Microstructure and mechanical properties of NbC-matrix hardmetals with secondary carbide addition and different metal binders, Int. J. Refract. Met. Hard Mater. 48 (2015) 418–426, https://doi.org/10.1016/j.ijrmhm.2014.10.014.

- [2] Y. Shao, Z. Guo, Y. Wang, H. Ma, Fabrication and characterization of NbC-CoCrFeNiMn high-entropy alloy cermets, Int. J. Refract. Met. Hard Mater. 94 (2021), https://doi.org/10.1016/j.ijrmhm.2020.105388.
- [3] Y. Zhao, L. Chen, J. Sun, W. Wu, T. Yu, Microstructure evolution and wear resistance of in-situ synthesized (Ti, Nb)C ceramic reinforced Ni204 composite coatings, Ceram. Int. 48 (2022) 17518–17528, https://doi.org/10.1016/j. ceramint.2022.03.016.
- [4] E. Gordo, F. Velasco, N. Antón, J.M. Torralba, Wear mechanisms in high speed steel reinforced with (NbC)p and (TaC)p MMCs, Wear 239 (2000) 251–259, https://doi. org/10.1016/S0043-1648(00)00329-X.
- [5] J. Xiong, Z. Guo, M. Yang, B. Shen, Preparation of ultra-fine TiCo.7NO.3-based cermet, Int. J. Refract. Met. Hard Mater. 26 (2008) 212–219, https://doi.org/ 10.1016/j.ijrmhm.2007.05.001.
- [6] M.B. Gilliard, B.T. Pierini, S.A. Alconchel, In situ formation of Fe-NbC/C composite powders from solution-derived precursors by a gas reduction-carburization process, Ceram. Int. 40 (2014) 14881–14889, https://doi.org/10.1016/j. ceramint 2014 06 083
- [7] L. Chen, T. Yu, P. Xu, B. Zhang, In-situ NbC reinforced Fe-based coating by laser cladding: simulation and experiment, Surf. Coating. Technol. 412 (2021), https:// doi.org/10.1016/j.surfcoat.2021.127027.
- [8] J.D. Avila, A. Bandyopadhyay, Niobium carbide reinforced-Ti6Al4V composites via directed energy deposition, Int. J. Appl. Ceram. Technol. 19 (2022) 1061–1073, https://doi.org/10.1111/ijac.13907.
- [9] X. Li, X. Yang, D. Yi, B. Liu, J. Zhu, J. Li, C. Gao, L. Wang, Effects of NbC content on microstructural evolution and mechanical properties of laser cladded Fe50Mn30Co10Cr10-xNbC composite coatings, Intermetallics 138 (2021), https://doi.org/10.1016/j.intermet.2021.107309.
- [10] J. Wang, C. Li, M. Zeng, Y. Guo, X. Feng, L. Tang, Y. Wang, Microstructural evolution and wear behaviors of NbC-reinforced Ti-based composite coating, Int. J. Adv. Manuf. Technol. 107 (2020) 2397–2407, https://doi.org/10.1007/s00170-020-05198-w
- [11] X. Li, Y. Feng, B. Liu, D. Yi, X. Yang, W. Zhang, G. Chen, Y. Liu, P. Bai, Influence of NbC particles on microstructure and mechanical properties of AlCoCrFeNi highentropy alloy coatings prepared by laser cladding, J. Alloys Compd. 788 (2019) 485–494, https://doi.org/10.1016/j.jallcom.2019.02.223.
- [12] Y. Zhang, M. Xiao, Y. min Zhou, Y. fu Shen, Microstructural transformation and tribological properties of laser-cladded FeNiCoCrTiO.5-xNbC high-entropy alloybased composite coatings, J. Therm. Spray Technol. (2022), https://doi.org/ 10.1007/s11666-021-01288-7.
- [13] Z. Chen, H. Yan, P. Zhang, Z. Yu, Q. Lu, J. Guo, Microstructural evolution and wear behaviors of laser-clad Stellite 6/NbC/h-BN self-lubricating coatings, Surf. Coating. Technol. 372 (2019) 218–228, https://doi.org/10.1016/j.surfcoat.2019.04.083.
- [14] Q. Li, Y. Lei, H. Fu, Growth characteristics and reinforcing behavior of in-situ NbCp in laser cladded Fe-based composite coating, J. Mater. Sci. Technol. 31 (2015) 766–772, https://doi.org/10.1016/j.jmst.2014.06.012.
- [15] X. Cai, L. Zhong, Y. Xu, Mechanical properties and tribological behavior of in situ NbC/Fe surface composites, J. Mater. Eng. Perform. 26 (2017) 292–299, https://doi.org/10.1007/s11665-016-2437-1.

- [16] B. Shi, S. Huang, P. Zhu, C. Xu, T. Zhang, Microstructure and wear behavior of insitu NbC reinforced composite coatings, Materials 13 (2020), https://doi.org/ 10.3390/MA13163459.
- [17] X.L. Ping, H.G. Fu, S.T. Sun, J. Lin, X.Y. Guo, Y.P. Lei, Microstructure and performance of Nb-bearing Ni60A-Cr3C2 coatings manufactured by laser cladding, Surf. Eng. 36 (2020) 1294–1306, https://doi.org/10.1080/ 02670844 2019 1631510
- [18] K. Wang, D. Du, G. Liu, B. Chang, J. Ju, S. Sun, H. Fu, Microstructure and property of laser clad Fe-based composite layer containing Nb and B4C powders, J. Alloys Compd. 802 (2019) 373–384, https://doi.org/10.1016/j.jallcom.2019.06.183.
- [19] Y. Bin Cao, H.T. Ren, C.S. Hu, Q.X. Meng, Q. Liu, In-situ formation behavior of NbC-reinforced Fe-based laser cladding coatings, Mater. Lett. 147 (2015) 61–63, https://doi.org/10.1016/j.matlet.2015.02.026.
- [20] H. Zhang, Y. Pan, Y. Zhang, G. Lian, Q. Cao, X. Zhu, Effect of NbC in-situ synthesis on the microstructure and properties of pre-placed WCoB-TiC coating by laser cladding, Int. J. Adv. Manuf. Technol. 120 (2022) 1265–1280, https://doi.org/ 10.1007/s00170-022-08844-7.
- [21] B. Lu, X. Cui, Y. Li, Z. Cai, E. Liu, G. Jin, Y. Hu, Microstructure, bonding properties and the basis of pinning effect of in-situ NbC reinforced Co50 composite coating by plasma cladding, Surf. Coating. Technol. 319 (2017) 155–163, https://doi.org/ 10.1016/j.surfcoat.2017.04.003.

- [22] G. Dong, B. Yan, Q. Deng, T. Yu, Effect of niobium on the microstructure and wear resistance of nickel-based alloy coating by laser cladding, Xiyou Jinshu Cailiao Yu Gongcheng/Rare Met. Mater. Eng. 40 (2011) 973–977.
- [23] J. Yang, J. Huang, D. Fan, S. Chen, Microstructure and wear properties of Fe-6wt.% Cr-0.55wt.%C-Xwt.%Nb laser cladding coating and the mechanism analysis, Mater. Des. 88 (2015) 1031–1041, https://doi.org/10.1016/j.matdes.2015.09.108.
- [24] W. Xi, B. Song, Z. Wang, T. Yu, J. Wang, Y. Dai, Effect of laser re-melting on geometry and mechanical properties of YCF102 cladding layer, Surf. Coating. Technol. 408 (2021), https://doi.org/10.1016/j.surfcoat.2020.126789.
- [25] Y. bin Cao, S. xin Zhi, Q. Gao, X. tao Tian, T. Geng, X. Guan, C. Qin, Formation behavior of in-situ NbC in Fe-based laser cladding coatings, Mater. Char. 119 (2016) 159–165, https://doi.org/10.1016/j.matchar.2016.08.005.
- [26] D. Pereira, J. Gandra, J. Pamies-Teixeira, R.M. Miranda, P. Vilaça, Wear behaviour of steel coatings produced by friction surfacing, J. Mater. Process. Technol. 214 (2014) 2858–2868, https://doi.org/10.1016/j.jmatprotec.2014.06.003.
- [27] S. Sun, H. Fu, X. Ping, J. Lin, Y. Lei, W. Wu, J. Zhou, Reinforcing behavior and microstructure evolution of NbC in laser cladded Ni45 coating, Appl. Surf. Sci. 455 (2018) 160–170, https://doi.org/10.1016/j.apsusc.2018.05.199.
- [28] Y. Bian, J. Ni, C. Wang, J. Zhen, H. Hao, X. Kong, H. Chen, J. Li, X. Li, Z. Jia, W. Luo, Z. Chen, Microstructure and wear characteristics of in-situ micro/nanoscale niobium carbide reinforced copper composites fabricated through powder metallurgy, Mater. Char. 172 (2021), https://doi.org/10.1016/j.matchar.2020.110847.